# Developing One-Part Alkali-Activated metakaolin/natural pozzolan Binders using Lime Waste as activation Agent

*Abdullah Kadhim[a, b] (a.m.kadhim@2017.ljmu.ac.uk), Monower Sadique [a] (M.M.Sadique@ljmu.ac.uk), Rafal Al-Mufti[a] (R.A.LatifAlMufti@ljmu.ac.uk), Khalid Hashim[a] (K.S.Hashim@ljmu.ac.uk),

(a) Department of Civil Engineering, Liverpool John Moores University, Henry Cotton Building, Webster Street, Liverpool L3 2ET, UK.

(b) Department of Civil Engineering, College of Engineering, University of Babylon, Babylon, Iraq.

## Abstract

Among the several schemes that have been reported to be a satisfactory alternative to Portland cement is Alkali Activated Cement (AAC), which has recently started to gain greater consideration in construction sectors. Conventional two-part alkali activation has many drawbacks, including the activating solution being viscous, problematic and non-user friendly to handle. Thus, this research aims to produce a one-part alkali activated metakaolin/natural pozzolan, by using an earth alkaline source (rich in CaO) from waste material (lime kiln dust), as an activating precursor to break the alumina-silicate crystalline phases. Thermal treatment of materials at two levels of treatment (450$^{o}$C and 950$^{o}$C), was used as an assisted activation approach. Analytical techniques including X-Ray powder diffraction XRD, Thermogravimetric Analysis TG-DTA, Fourier Transform Infrared Spectroscopy FTIR and Scanning Electron Microscope SEM, were utilised to investigate the performance of the developed materials at a molecular level. Reduction of crystalline peaks as well as the appearance of new wollastonite minerals within the calcined lime kiln dust, contributed to the development of 27 MPa compressive strength after 28 days. The dissolution made through the pozzolanic reaction as well as thermal treatment evidently contributed to transform crystalline to amorphous phases.

## Keywords

Alkali-activated cements , Lime, Thermal behaviour, , Diffraction (X-ray, neutron, electron), Thermal analysis, Infrared (R, FTIR).

# 1. Introduction

The world production of the Ordinary Portland Cement (OPC) is growing and reached 4.1 billion metric tonnes in 2018(U.S. Geological Survey, 2019). The use of Portland cement in concrete construction is under serious evaluation, because of substantial challenges that are facing the method of production for conventional cement. Firstly, the energy consumption through the whole process. Secondly, the high quantity of carbon dioxide gas ($CO_2$) is released to the atmosphere through the production of cement (Demie *et al.*, 2013). Alternatively, there are noteworthy investigations to develop other types of cements that are entirely free of (OPC) and based principally on green raw materials. Mineral Products Association (MPA) in the UK, listed a number of novel (non-Portland) cements with low energy in their fact sheet (Mineralproducts.org, 2017). One of these novel cements is Alkali Activated Cement (AAC). AACs are cementitious materials, formed as a result of an alkaline reaction with amorphous or vitreous alumina-silicates. When mixed with alkaline activators (solid or liquids) in a chemical reaction called alkali-activation or alkalination, these materials set and harden, yielding a material with good binding properties (Davidovits, 1993; Provis, 2017). Conventional two-part alkali activation (wherein a solid raw material is activated with alkaline chemical solution) has many drawbacks: the hazardous activating solution, which makes it non-user friendly to handle. On the other hand, the activator solutions of alumina-silicate material represents a real concern through the use of (AAC). The activator solutions provide the highest single contribution to the embodied carbon dioxide of (AAC) (Van Deventer *et al.*, 2012; Provis *et al.*, 2015; Luukkonen *et al.*, 2018). Until now, it cannot be said that (AAC) are based on friendly and environmentally friendly process, as the production of the chemical solutions releases large amounts of $CO_2$ to the environment (Torres-Carrasco *et al.*, 2017).

Several efforts have been made to develop a one-part alkali activated cement (AAC) which can be found under different terminology in the literature, such as one-part alkali activated cement, self-activating cement or one-part alkali alumina-silicate hydraulic cement (Matalkah *et al.*, 2016; Almalkawi *et al.*, 2017; Ban *et al.*, 2017). In one-part mixtures, only a dry mixture is needed in addition to water. The dry mixture is prepared by mixing a solid alkali-activator with a solid alumina-silicate precursor, with or without an assisted activation approach (Matalkah *et al.*, 2016; Luukkonen *et al.*, 2018; Abdel-Gawwad *et al.*, 2019).

Provis (2014), defined the activators as any substance that represents an alkaline source that raises the pH of the reaction mixture and simplifies dissolution. This includes alkali cations ($Na^+$, $K^+$) or earth alkaline cations ($Ca^{+2}$, $Mg^{+2}$). A substantial number of published studies that explored the synthesis of one-part (AAC), have used alkaline commercial solid chemical activators, including primarily sodium hydroxide (NaOH) aided by other chemical agents to improve the alkalination in binder such as sodium silicates ($Na_2SiO_3$), sodium carbonates ($Na_2CO_3$). Realistic reports revealed that these chemicals are expensive and primarily contribute to the total cost of production of (AAC) cost (Weerdt, 2011; Van Deventer *et al.*, 2012; Heath *et al.*, 2013; Kim *et al.*, 2013).

Therefore, using solid chemicals do not represent a realistic commercial or environmental optimal solution that can be used as an activator (Luukkonen *et al.*, 2018).

Previous studies have reported on the use of (CaO) and $Ca(OH)_2$ as potential alternative activators, as these activators are cheaper than (NaOH or $Na_2SiO_3$ ) (Kim *et al.*, 2013; Vaccari *et al.*, 2013). For instance, the total cost of NaOH is nearly 5-6 times higher than that CaO global (Vaccari *et al.*, 2013) These activators provide alkaline earth cations in place of alkali cations, which ease the creation of different binding phases, when compared to blends of low calcium content (Li *et al.*, 2010; Luukkonen *et al.*, 2018). An earlier study by Cabrera and Rojas (2001) investigated the metakaolin-lime-water system by thermal analysis. The study confirmed the appearance of reaction products encompassing principally Strätlingite ($C_2ASH_8$) and tetra calcium aluminium hydrate ($C_4AH_{13}$) as the reason for binder strength development. Kim et al. (2013), used commercial (CaO) solid powder to produce non-cement binder, with ground granulated blast furnace slag as the Si/Al source material. When compared to $Ca(OH)_2$, CaO activator was noticed to provide a higher mechanical strength up to 53 MPa at 56 days due to the production of more (C-S-H) than $Ca(OH)_2$. Nevertheless, when investigating the energy and ecological analysis of synthesising high purity chemical CaO powder, it was discovered that the synthesis process has high energy consumptions and a complicated process requiring a high level of accuracy(Licht, 2016)('Production of purified calcium carbonate', 1993). Different activation assisted methods were used in the production of one-part (AAC). Thermal activation (calcination) was used recently as an assisted approach to improve the reactivity and the amorphicity of supplementary cementitious materials, such as natural pozzolans (Almalkawi *et al.*, 2017; Abdel-Gawwad and Khalil, 2018). During the thermal treatment of material, crystalline bonds are broken down and transformed to a glassy or amorphous phase resulting in a more reactive binder.

The principal aim of this work is the development of novel approach to produce a one-part (AAC) without the need to the presence of commercial chemical activator. This will be achieved by providing the earth alkaline source from a by-product waste material, which is primarily composed of reactive (CaO). This by-product results from the production of quick lime known as lime kiln dust (LKD), which is regularly disposed of in landfills worldwide. For instance, in the USA, it is estimated that about 2.5 million metric tonnes of high-calcium LKD is produced annually(Miller *et al.*, 2004). Thus, LKD requires reuse, in order to lessen environmental problems and promote sustainability. LKD is mainly composed of a CaO compound and high alkaline materials (high pH). Presence of reactive CaO in material with high quantities contributes to raise the alkalinity scale (PH) in which is leading to high level of dissolutions. This was proved by past studies that used materials of CaO to enhance the reactivity of binder matrix such (Kim *et al.*, 2013; Vaccari *et al.*, 2013). Other studies used even OPC as a source for CaO to improve the properties of their developed products such Nath and Sarker (2015).

A combination of metakaolin, which is the crystallographically disordered layered product of dihydroxylation of kaolinite (an alumina-silicate clay) (Rashad, 2013; Provis *et al.*, 2014) and volcanic tuff or natural pozzolan were used as an alumina silicate (Al/Si) source to formulate one-part dry AAC powder that just needs water to produce the binding material. Volcanic tuffs, provide

an extensive variety of reactivity, dependent upon their degree of crystallinity and mineralogy. The proposed Alumina-silicate precursors, undertake dissolution and precipitation processes when mixed with lime or CaO, yielding calcium alumina-silicate hydrate (C-A-S-H) (Nath *et al.*, 2015).

As for the traditional method (with alkaline chemicals) of producing AAC, in addition to the related health and safety concerns which increase the production cost, there is a limited production capacity of these chemicals as they need high accuracy and huge plants. For instance, sodium hydroxide (NaOH) is currently produced at approximate rate 60 Mt per year via the chlor-alkali process and up-scaling this production is not straightforward because chlorine ($Cl_2$), which has a limited world-market, is produced as a side-product (Provis, 2017; Luukkonen *et al.*, 2018). Therefore, replacing synthetic alkali silicates with other alkali and silica sources is important.

Hence, this study represents an attempt and evaluation of the performance of one-part (AAC) comprised from a combination of (Al/Si) activated by waste material rich of (CaO). Thermal treatment was used as an assisted activation method to increase the reactivity and amorphicity of raw materials. Materials were characterised in terms of their physical, chemical, metallurgical and thermogravemetrical properties to reveal the changes after thermal treatment.

# 2. Materials and methods

## 2.1 Materials used

The proposed materials were collected from various suppliers in the UK to ensure their local availability . The alumina-silicate source was produced by combination of metakaolin (MK) and a volcanic tuff or natural pozzolan (NP) which were supplied by two commercial suppliers. For improved alkalinity within the blended system, lime kiln dust (LKD) was used that was also supplied by a waste producing industry in the UK. The proposed materials were assessed and characterised to evaluate their physico-chemical properties and have been tabulated in Table 1 below. The specific surface area was determined by air permeability test (Blaine method) which is described in BS EN 196-6 (2010).

*Table 1. Physical properties of undisturbed materials.*

| Material | Specific surface area (Blaine) ($cm^2/g$) | pH | Density ($g/cm^3$) |
|---|---|---|---|
| MK | 196000 | 6 | 2.69 |
| NP | 172000 | 6 | 2.57 |
| LKD | 101000 | 12.3 | 2.7 |

Particle size distribution (PSD), was determined by Beckman Coulter laser diffraction particle size analyser as shown in Figure. 1. MK and NP were identified as having similar size distributions with ($D_{50}$) being 9.22, 7.87µm respectively. Conversely, LKD was found to be coarser with a ($D_{50}$) 15.94µm. This particle size range of raw materials has high positive effect on alkali activation reaction. Rashad (2016), reported that as the grain size is lower than 32 µm of MK, providing workable mix with higher compressive strength.

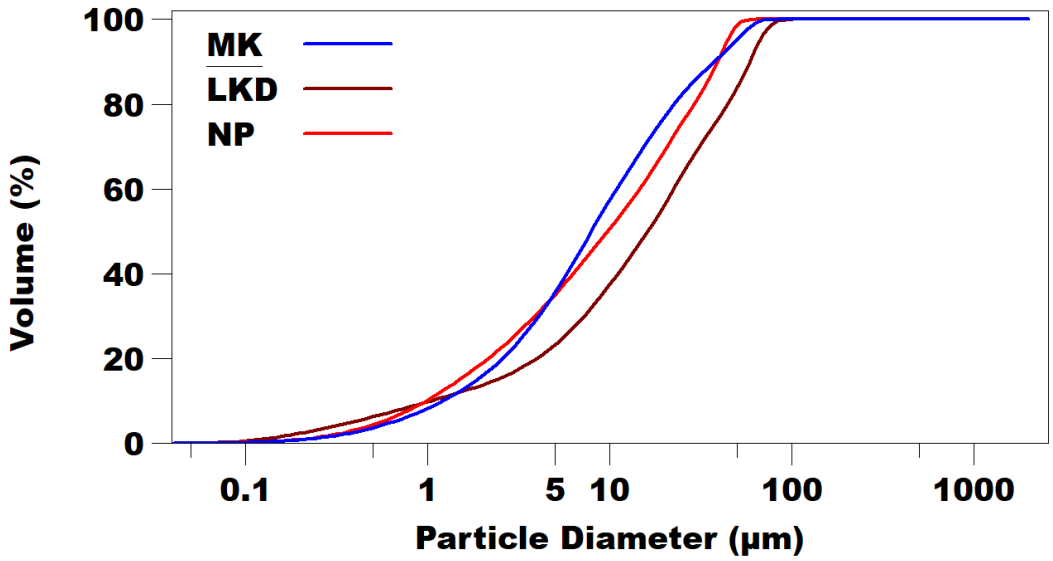


*Figure 1. Particle size distribution (PSD) of starting materials.*

The elemental composition of raw materials was determined, as they were received using a Shimadzu EDX 720, energy dispersive X-ray fluorescence (EDXRF) spectrometer. The key oxide elements are listed in Table 2. It is shown that MK and NP are mainly composed of $SiO_2$ and $Al_2O_3$, which can be considered as an ideal source of siliceous and aluminate materials, with minor quantities of CaO, $Na_2O$, $K_2O$ and MgO in NP. LKD is mostly rich in CaO of 80.1Wt.% with slight amounts of $SiO_2$ and $Na_2O$, therefore it was considered as calcareous source.

*Table 2. Chemical composition by XRF of raw materials (Wt.%).*

| Components (wt. %) | $SiO_2$ | $Al_2O_3$ | $Fe_2O_3$ | CaO | $Na_2O$ | $K_2O$ | MgO | $TiO_2$ |
|---|---|---|---|---|---|---|---|---|
| **MK** | 55 | 40 | 1.4 | 0.15 | 0.4 | 0.4 | 0.95 | 1.7 |
| **NP** | 46.6 | 30.4 | 3.8 | 4.5 | 3.9 | 6 | 4.2 | 0.6 |
| **LKD** | 14.6 | 0.2 | 0.1 | 80.1 | 3.8 | 0.5 | 0.6 | 0.1 |

## 2.2 Characterisation Methods

In order to further investigate the behaviour and the performance of the materials and assess their chemical mineralogy and microstructure, the following characterisation techniques have been utilised:

### 2.2.1 Energy-Dispersive X-ray diffraction (EDXRD)

X-ray diffraction (XRD), is the elastic scattering of x-ray photons by atoms in a periodic lattice. The scattered monochromatic x-rays that are in phase, produce constructive interference (Ramachandran *et al.*, 2000). XRD was used in this research to determine the amorphous content and the mineralogy phases of each material. The test was carried out using a Rigaku mini-flex diffractometer (mini-flex goniometer), with CuK X-ray radiation (30 kV voltage and 15mA current at scanning speed of 2.0deg./min in continuous scan mode) and scanning range: $2\theta = 5–65°$. XRD was investigated for the raw materials before and after thermal treatment at (950$^{o}$C and 450$^{o}$C). Moreover, a small sample of each (AAC) hydrated and hardened paste were finely grinded, dried, and at age of 28 days investigated via XRD analysis for mortars with the highest strength.

### 2.2.2 Thermogarvemetric Analysis (TGA)

Thermal analysis, is used to monitor the mass of material as a mean of temperature or time as the sample specimen is subjected to a controlled temperature program, in a controlled atmosphere. Thermal analysis used in this investigation, consisted of Thermogarvemetric analysis (TG), which usually determines thermal events related to weight loss of the sample. However, this technique does not detect phase change, such as “melting”; and differential thermal analysis (DTA) is employed, which is the first derivative of the weight loss curve. DTA indicates phase changes as endothermic and exothermic peaks (Hill *et al.*, 2019). Therefore, it is donated as TG-DTA technique. The tests were completed using the Perkin Elmer TGA Q50 V20.13 Build 39. The thermal performance of materials was investigated by TG-DTA, with a heating range 20-900$^{o}$C and a heating rate 10 $^{o}$C/min. In this study, TG-DTA investigations were performed for raw materials to assess their thermal behaviours during individual calcination.

### 2.2.3 Fourier Transform Infrared Spectroscopy (FT-IR)

FT-IR, represents a supplementary technique for the assessment of elemental compositions, chemical bonds and molecular vibrations of samples. Infrared (IR) radiation is distributed over a sample. In this investigation, FT-IR was conducted for raw materials and for hardened pastes at age of 28 days for specimens of the highest strength. FT-IR analysis was carried out by using a Perkin-Elmer Spectrum BX series Fourier transform infrared spectrometer (FT-IR), equipped with a Miracle ATR accessory (Specac, UK). The spectrum of the sample was recorded by accumulating 16 scans at 4cm$^{-1}$ resolution and wavelength between (524cm$^{-1}$ and 2000cm$^{-1}$).

### 2.2.4 Scanning Electron Microscope (SEM) & Energy Dispersive X-rays Spectroscopy (EDX)

SEM morphological analysis and observations were conducted for raw materials and hardened pastes at age of 28 days . EDX is an analytical system where element specific radiation is used for chemical characterisation of the surface near volume. With the aid of proper detectors, the energy or the X-rays are determined. EDX, when combined with SEM, provides elemental analysis on areas as small as nano-metres in diameter. In this study, EDX-SEM was conducted using an Oxford Inca x-act detector (45nA prob current and 100 sec counting time) and a FEI SEM model Inspect S(20kV accelerating voltage) for hardened pastes at age of 28 days. One day before the 28 days, pastes were removed from water curing and left to dry in room temperature air (20$^{o}$C). This step was conducted in order to avoid coating with gold when performing EDX as this might affect the spectrum elemental analysis.

### 2.2.5 Compressive strength

The compressive strength of mortar prisms, was based as a function for evaluating the mechanical properties of specimens and was measured according to the standard BS EN 196-1 (2016). The test was carried out by a Control Automax 5 compression tester, with a load rate of 0.4 MPa/sec.

## 2.3 Characterisation of materials

The XRD, SEM, FT-IR and TG-DTA analysis of undisturbed materials has been illustrated in Figures 2 to 5. From the X-Ray diffractions of MK as shown in Figure. 2, it is observable that MK comprises many crystalline phases and is primarily composed of quartz ($SiO_2$), and (Mullite $Al_6Si_2O_{13}$) in major crystalline peaks.
Kaolinite ($Al_2Si_2O_5$ (OH) $_4$) and Illite ($K,H_3O)(Al,Mg,Fe)_2(Si,Al)_4O_{10}[(OH)_2,(H_2O)]$ compounds in minor peaks. Highest quartz peak was at (2θ) 26.73$^{o}$. Diffractogram pattern of NP, which has closely crystalline peaks with the highest quartz peak at (2θ) 26$^{o}$. Smaller peaks are formed by feldspars such as Anorthite ($CaAl_2Si_2O_8$) and Clinoptilolite ($KNa_2Ca_2$ ($SiO_{29}Al_7$) $O_{72}$ $24H_2O$). Moreover, Edenite ($Ca_2NaMg_5$ ($AlSi_7$) $O_{22}$ (OH) $_2$) was present in NP diffractions with high quantities. Diffractions of LKD show one recognised crystalline peak of lime (CaO) a with high intensity. Smaller peaks exist in forms of quartz ($SiO_2$), Natrosilites ($Na_2Si_2O_5$) and Ertixiite ($Na_2Si_4O_9$). The presence of such compounds, increases alkalinity activity in LKD, which are similar to the content of water glass ($Na_2SiO_3$) commercial activator.

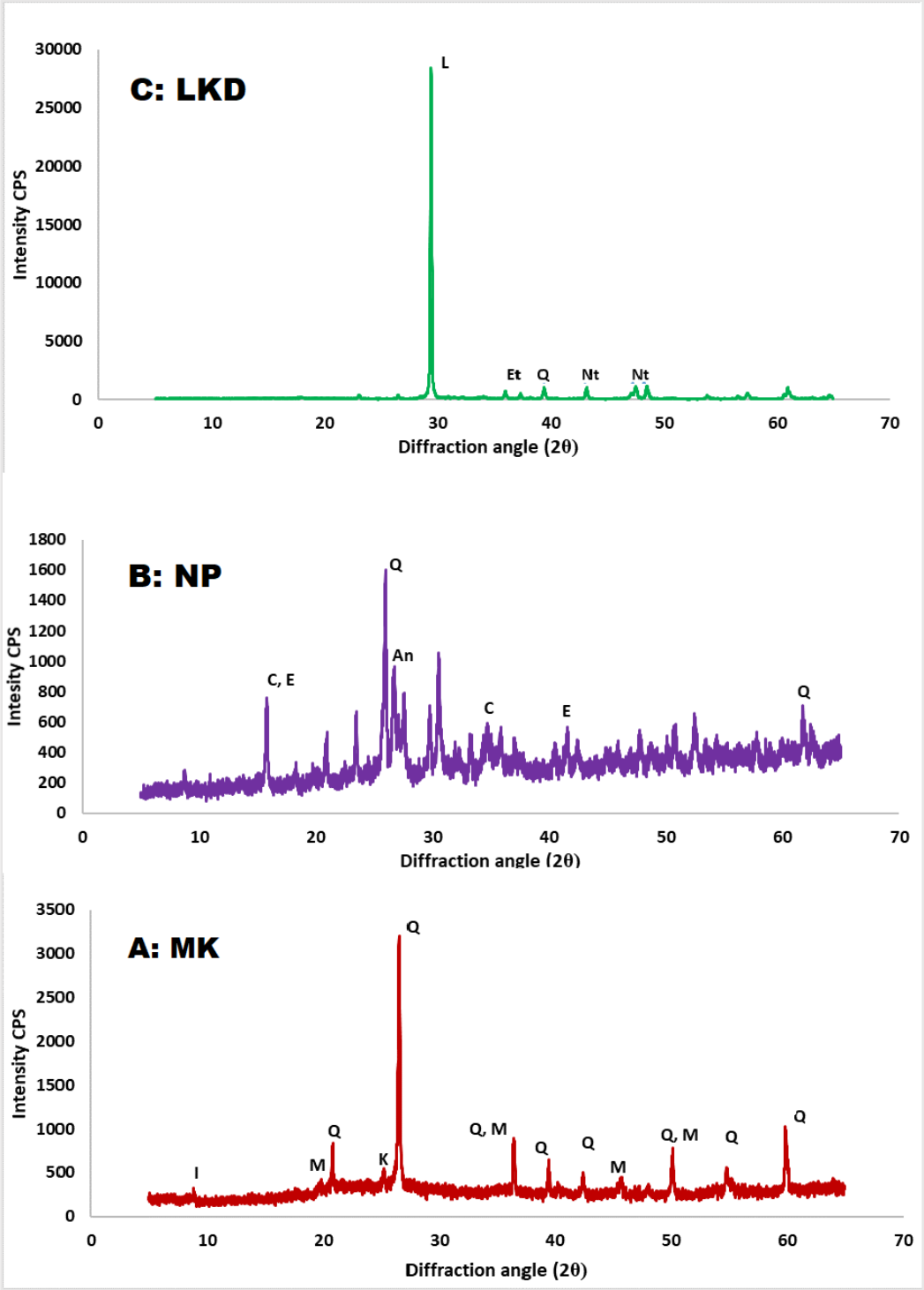


*Figure 2. XRD-patterns of initial materials*

*Q: Quartz, K: kaolinite, M: Mullite, I: Illite, C: Clinoptilolite, An: Anorthite, E: Edenite, L: Lime, Nt : Natrosilites, Et: Ertixiite.*

Scanning electron microscope images illustrating the particles of original materials, as shown in Figure. 3. MK, seems to have fine and lamellar particles with random non uniform shapes. Particles of LKD look coarser and have less surface area with flaky shapes. The raw NP particles, as shown in the SEM image, are irregular in shape and size.

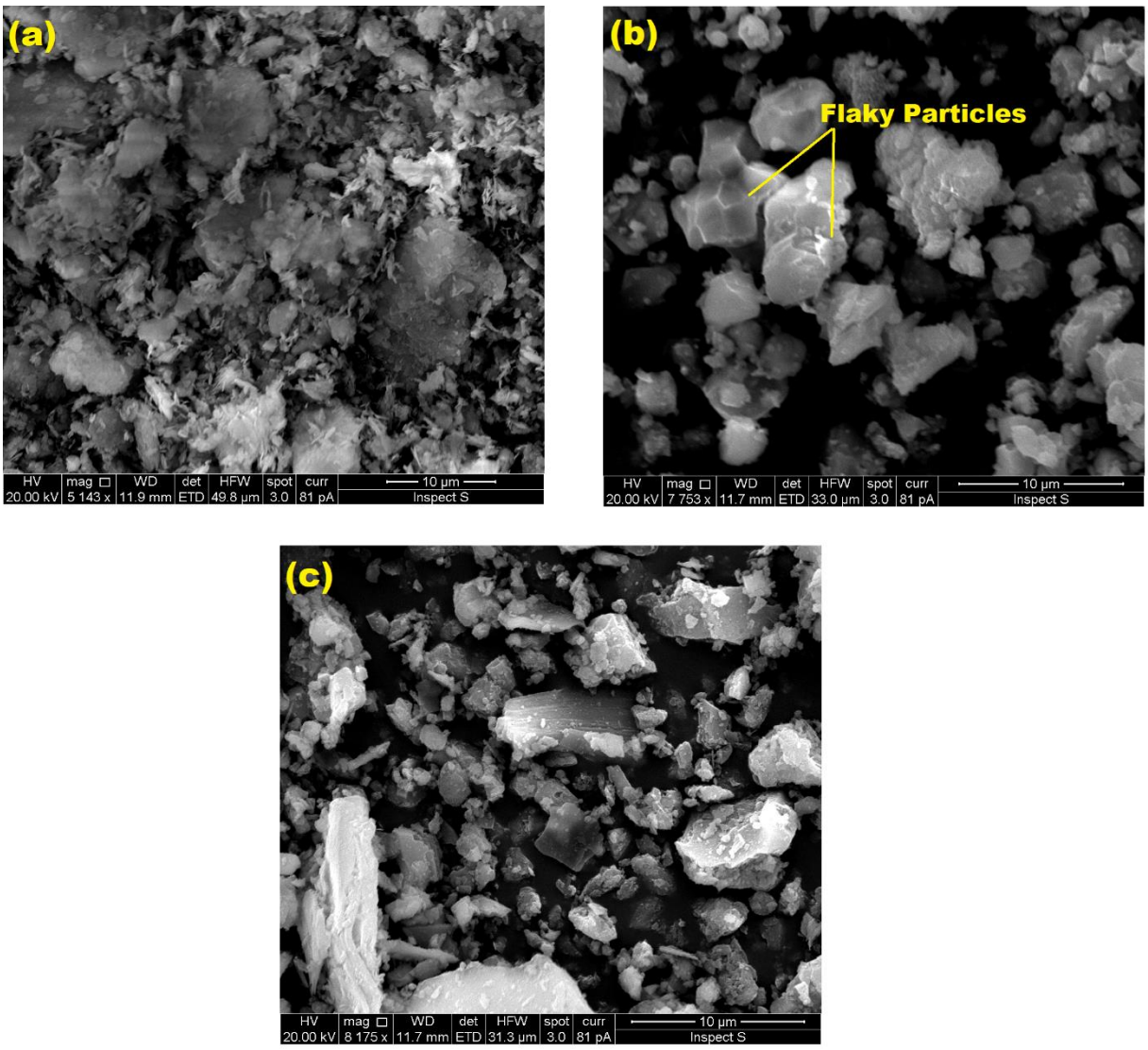


*Figure 3. SEM micrographs of a) MK, b) LKD and c) NP.*

In Figure. 4 , FT-IR measurements of raw MK and NP are indicating the that highest absorption bands at 1046 $cm^{-1}$ and 996 $cm^{-1}$ respectively, which were attributed to the strong bands of Si–O–Al and tetrahedral Si–O–Si of bridging oxygen (BO) atoms of the original alumina-silicate framework (Vizcayno *et al.*, 2010). The characteristic peaks appearing at 794$cm^{-1}$ and 724$cm^{-1}$, are ascribed to the stretching vibration Si–O and stretching Al 6-coordinated geometry (AL, Mg)–O–OH (Nayak *et al.*, 2007). Both absorptions Si–O–Si and Si–O, are supporting the presence of quartz, while Si–O–Al is supporting the presence of kaolinite (Kakali *et al.*, 2001; Nayak *et al.*, 2007). These peaks are related to the alumina-silicate prevalence phases in both MK and NP. The

strong presence of calcite ($CaCO_3$) presented by the C–O bond, was evidently presented by the bands at 1402, 872 and 712$cm^{-1}$ (Miguel *et al.*, 2009). The presence of these bands are accredited to the tendency of CaO to react naturally with $CO_2$ in the atmosphere.

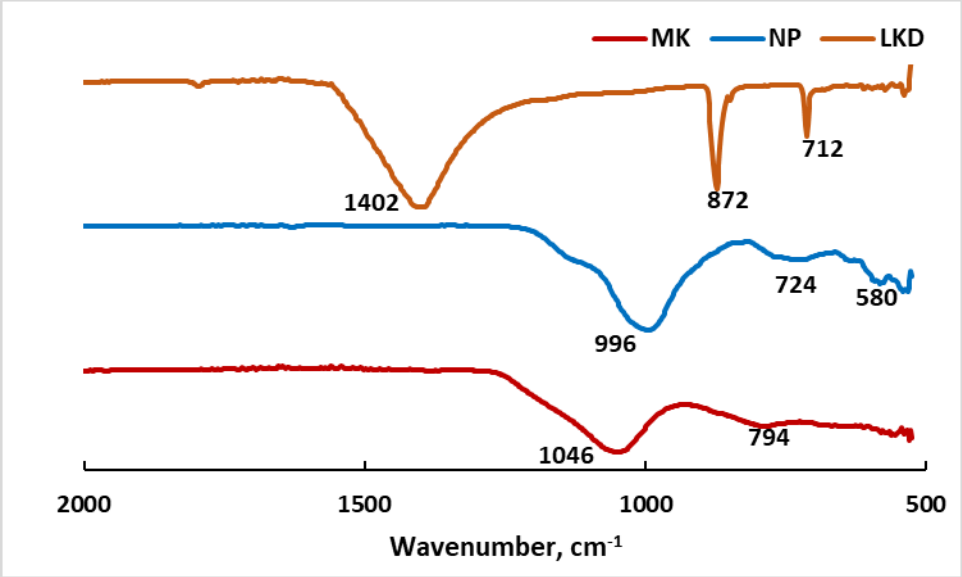


*Figure 4. FTIR-spectra of Raw MK, NP and LKD*

Figure. 5A exhibits the thermal performance of NP investigated by TG-DTA, when calcined to 900$^{o}$C. As can be seen, some mass-loss phases are present in its patterns caused by endothermic and exothermic reactions. The thermogravemetric (TG) patterns of NP mass-loss from room temperature to 900$^{o}$C is approximately 7% of the total weight , which might be attributed to the loss of chemically and physically adsorbed water and breakdown of crystal phases, which was evidenced by XRD analysis. The loss of weight can be divided into three stages. The loss from 20-320$^{o}$C is due to the evaporation of adsorbed water. The loss from 320 – 620$^{o}$C, is because of calcining amounts of impurities and contaminants. While loss from 620 to 900$^{o}$C is due to decomposition of unburnt carbons (Duxson *et al.*, 2007; He *et al.*, 2010). As for the DTA curve, there was endothermic convexity at 119 $^{o}$C, which relates to the evaporation of water followed by exothermic concavity at 250$^{o}$C. The TG curve of MK has shown a very small weight change within 2% of the total weight, with a reasonably straight DTA curve, as shown in Figure. 5B. The TG patterns of LKD have revealed that it has not lost any weight until 350$^{o}$C; with there was slight weight loss. While the peak which starts from 600 $^{o}$C and ends with 750 $^{o}$C, the weight changed dramatically with a 40 % loss of original weight and an exothermic sharp peak of the DTA curve, which is shown clearly in Figure. 5C. This loss is markedly attributed to the transformation and loss of the CaO crystalline intense peak, which was further evidenced by the XRD analysis of 950$^{o}$C calcination, when this peak disappeared from the diffraction pattern.

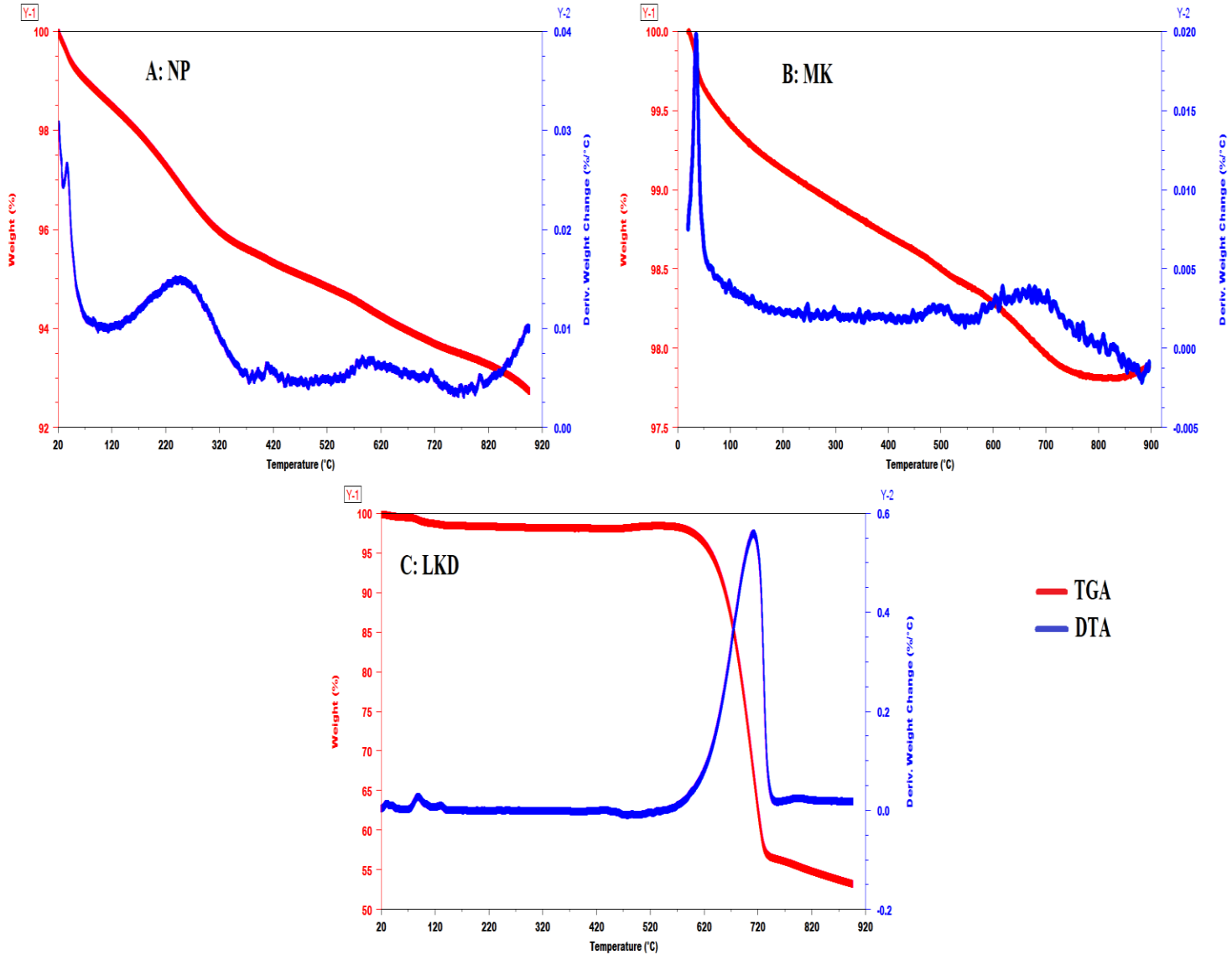


*Figure 5. TG-DTA curves of A: NP, B: MK, C: LKD*

## 2.4 Alkaline activated cement (AAC) synthesis

### 2.4.1 Thermal activation

Thermal treatment or calcination, means heating the substance to high temperature (500-2000$^0$C) within a controlled atmosphere, in order to increase their reactivity by changing their mineralogy. Thermal treatment is used as one of the assisting activation methods to produce one-part (AAC) cement. Most of the materials, which are clayey in origin, require calcination in order to be reactive. For instance, metakaolin ($Al_2Si_2O_7$) is originally synthesised from the calcination of kaolin clay ($Al_2SiO_5$ $(OH)_4$) (Ilić *et al.*, 2010). During the calcination process, dihydroxylation is carried out, leading to the loss of the long-range order of alumina and silica layers and conversion of the powder to an amorphous form. Another change is that the alumina transforms from the octahedral coordination to tetrahedral coordination, due to calcination (Justnes *et al.*, 1990). Thermal activation was performed for the materials individually to increase their reactivity and to evaluate the effect of each calcined material on the blended properties. Subsequently, mixing each calcined material with the other two non-calcined precursors according to the blending concept (Si/Al+alkaline) was carried out to synthesise a dry hydraulic cement, as illustrated in Figure. 6. Thermal treatment was conducted in a muffle furnace with a ramping temperature of 20 $^0$C/min for 2 hours. Two foundry cylindrical silicon carbide graphite crucibles (500ml) and two alumina cylindrical crucibles (175ml), were used during calcination. It was stated from past studies that crystallinity and reactivity of most materials rich in alumina-silicate content can increase with temperatures up to 750 -1200$^o$C and after this temperature range, their reactivity can be decreased (Sanz *et al.*, 1988; Yao *et al.*, 2009; Davidovits, 2017; Peng *et al.*, 2017). However, Davidovits (2017) stated that the intensity line of the most reactive Al species existed in MK, Al(5) and Al(4) are becoming very well defined at temperature 900 $^o$C for 4 hours calcination time. Therefore, 950 $^o$C for 2hours was used in this study for MK calcination.

In this study activation at 450 $^o$C temperature at mid-range between 0 and 950$^o$C was also investigated to evaluate and compare the phase transitions. Noteworthy that during treatment some of the material colours have changed in both stages of temperatures. MK was becoming whiter as increasing temperature as shown in Figure. 6. NP has shown considerable changing from greyish colour to brown as high as temperature. The colour transformation of NP attributed to the increment of anorthite mineral that been observed clearly in XRD patterns which turned to be brown in nature(Kimata *et al.*, 1996). LKD originally white but turned with a little greyish at 950$^o$C.

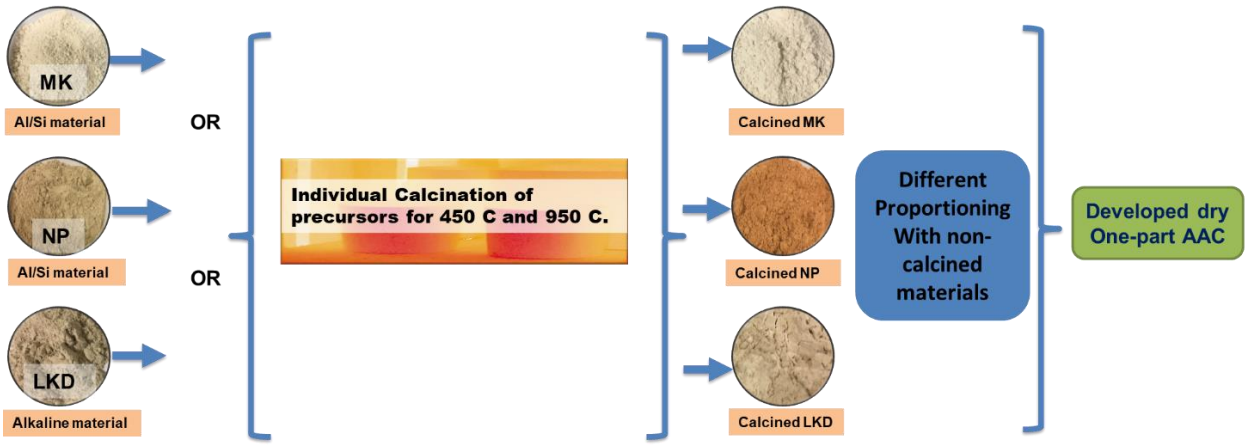


*Figure 6. Preparation steps of one-part (AAC)*

### 2.4.2 Formation of hydraulic cement mortar

CEN standard kiln dried sand in accordance with BS EN 196-1 (2016) and supplied from (Tarmac) was used in mortars with particle size distribution shown in Figure. 7 and a specific gravity of 2.62 g/cm$^3$ with binder to sand ratio is (1:2). The mixing procedure was followed according to the requirements of BS EN 196-1 (2016). Initially, 0.55 water/binder ratio was chosen, but it was found that the mortars were extremely workable therefore; it was reduced to 0.45 for all the mortars, where appropriate consistency was achieved at this stage.

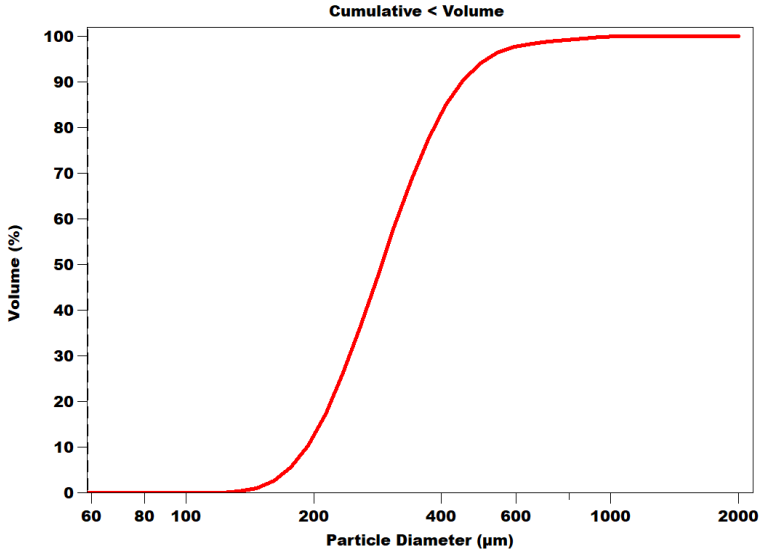


*Figure 7 Particle Size Distribution of the used sand*

Initially, raw materials were mixed before treatment based on their chemical elements to form (Al/Si) + alkaline system. Based on this, the formulation designs of materials were as shown in Table 3. Firstly, MK and LKD (50M50L) were mixed with 50% each to evaluate the strength

obtained from the combination. Compressive strength was tested on 7, 14 and 28 days of the mixes. This step was conducted to find out which materials gathering are making the highest strength.

*Table 3. Initial mixes proportion*

| Mix ID | Binder contents |
|---|---|
| 50M50L | MK 50% LKD 50% |
| 75M25L | MK 75% LKD 25% |
| 25M75L | MK 25% LKD 75% |
| 25M65M10N | MK 25% LKD 65% NP 10% |
| 40M40L20N | MK 40% LKD 40% NP 20% |

However, the compressive strength of these initial mixes as shown in Figure 8 below does not show significant strength except (25M75L) which is 20 MPa at age 28 days. The attempt of optimising this mix by the inclusion of 10% and 20% of NP as (25M65M10N and 40M40L20N) in the above table has caused sharp reduction in strength at this stage as shown in Figure 8.

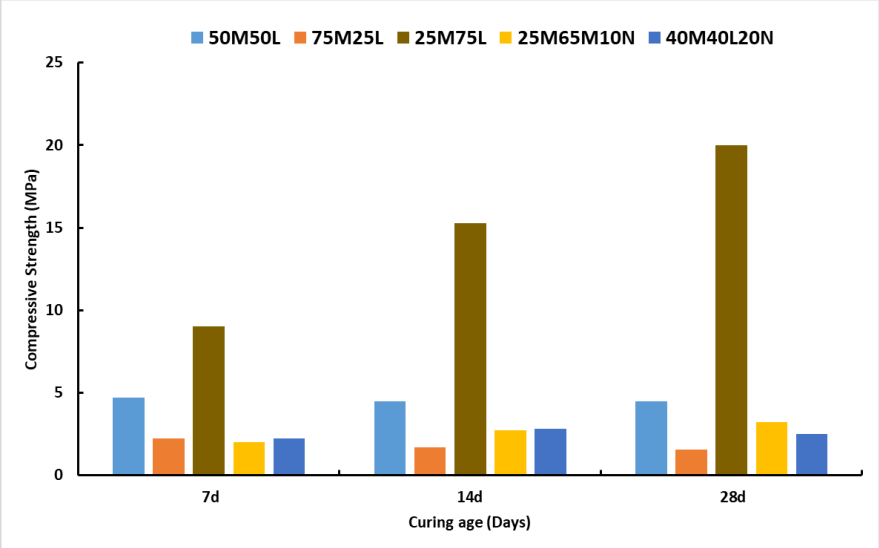


*Figure 8. Compressive strength of initial mixes*

The optimum mix from the initial stage with no thermal treatment was mix of (25M75L). This mix was investigated for thermal treatment with both of its components have been calcined individually but did not provide change of strength compared to the state of no thermal treatment. However, the only considerable change was noticed when NP was added of 20% and 30% with calcined LKD was reduced to 40% and 30% as illustrated in the results of 40M40(L-950)20N and 35M35(L-950)30N respectively.

The dry one-part AAC powder mixes were blended in ternary process as shown below in Table 4 with different mix compositions. The dry powder was mixed in mechanical mixer (Hobart 5 litre mixer) for 3 minutes to homogenise the mixture. Afterward, the tap water and sand were added respectively and the mixing of mortar is carried out to obtain a uniform mortar mixture. The blended mortars were casted in steel prism moulds (40 mm × 40 mm × 160 mm). After 24 hour, the hardened specimens were demoulded and were cured in a hot water curing regime to enhance the reactivity and the hydration rate of the mortars. In mortars activated with alkaline chemicals in which mainly consisting of Sodium hydroxide (NaOH), there is high possibility that the produced system to suffer problems of efflorescence, micro cracking as a result of dehydration which causes decrease in compressive strength (Li *et al.*, 2013). The need for relative humidity is mainly to tackle the aforementioned issues with systems made of chemicals as high levels of heat are generated as a result of sodium species dissolution which lead to cracks (Peng *et al.*, 2017). In this study, hot water is mainly used for accelerating and promoting the hydration reactions during the curing period. Curing temperature was fixed to 50 $^{o}$C for 7 days and then cured in normal 20 °C water until 28 days as suggested by Perera (2007) and Singh (2015).

*Table 4. Mixing proportions of blends.*

| Mix ID | Binder contents | Calcination temperature ($^{o}$C) | Calcined constituent |
|---|---|---|---|
| 40M40L20(N-950) | 40%MK 40%LKD 20%NP | 950 | NP |
| 40(M-950)40L20N | 40%MK 40%LKD 20%NP | 950 | MK |
| 40M40(L-950)20N | 40%MK 40%LKD 20%NP | 950 | LKD |
| (40M40L20N)-950 | 40%MK 40%LKD 20%NP | 950 | NP, MK, LKD |
| 35M35L30(N-950) | 35%MK 35%LKD 30%NP | 950 | NP |
| 35(M-950)35L30N | 35%MK 35%LKD 30%NP | 950 | MK |
| 35M35(L-950)30N | 35%MK 35%LKD 30%NP | 950 | LKD |
| (35M35L30N)-950 | 35%MK 35%LKD 30%NP | 950 | NP, MK, LKD |
| 35M35L30(N-450) | 35%MK 35%LKD 30%NP | 450 | NP |
| 35(M-450)35L30N | 35%MK 35%LKD 30%NP | 450 | MK |
| 35M35(L-450)30N | 35%MK 35%LKD 30%NP | 450 | LKD |
| (35M35L30N)-450 | 35%MK 35%LKD 30%NP | 450 | NP, MK, LKD |

# 3. Results and discussion

## 3.1 Effect of thermal treatment on mineralogy

The powder diffraction of calcined materials has been shown in Figure. 9. Diffractograms of MK, have revealed a significant reduction and even disappearance of kaolinite and quartz peaks after both levels of calcination indicating semi-transformation of material to an amorphous phase.

XRD spectrums of calcined NP at both levels, indicated a huge transformation of crystalline phases to amorphous phases through the loss of quartz and clinoptilolite, in a range of 2θ from 30 º to 60º. It can be noticed, that crystalline quartz peak at 2θ = 26º has disappeared entirely when NP calcined to 450ºC and 950ºC, introducing strong evidence of the increment of amorphicity. This was confirmed by the formulation of a broad amorphous hump of anorthite existed at 2θ = 26.7º and 2θ = 27.8º at 950ºC patterns. Remarkably, this intense peak in LKD was diminished markedly when calcined to 450ºC and completely disappeared in 950ºC calcination. The appearance of new diffraction patterns at new angles of calcined LKD at 950ºC, indicated formation of the new compounds, but was composed of the same elements as untreated LKD (CaO, $SiO_2$ and $Na_2O$) in the form of wollastonite minerals; dectolite ($NaCa_2Si_3O_8(OH)$) and dellaite ($Ca_6Si_3O_{11}(OH)_2$) (Eilers *et al.*, 1983; Garbev *et al.*, 2008). This was accompanied by the complete disappearance of the intense crystalline CaO at 950ºC calcination, which indicated that calcination had caused a large combination of lime CaO with the compounds of $SiO_2$ and $Na_2O$, to form the above compounds.

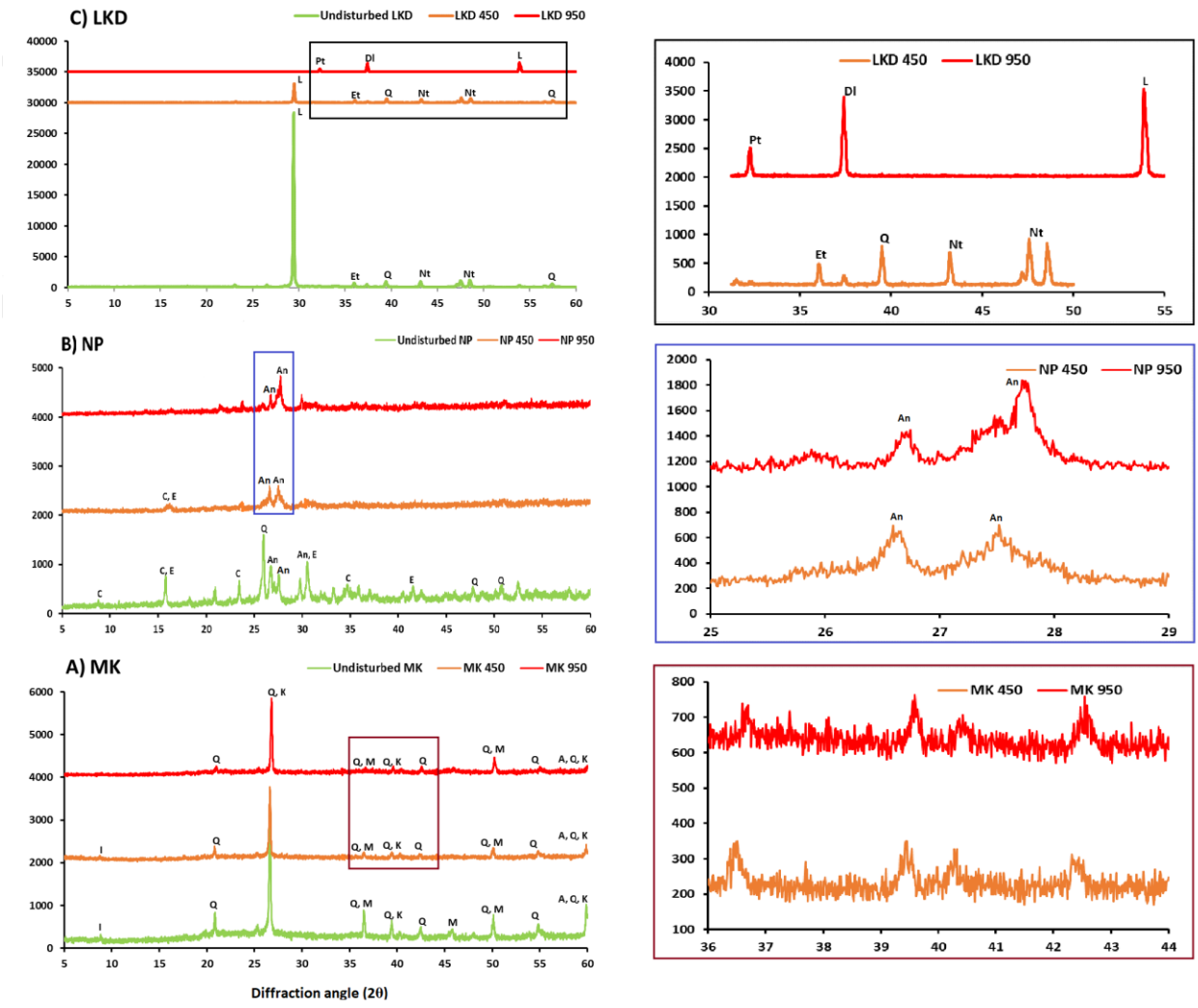


*Figure 9. XRD patterns of materials after thermal treatment A)MK, B)NP, C)LKD.*

*Q: Quartz, K: kaolinite, M: Mullite, A: Anatas, I: Illite, C: Clinoptilolite, An: Anorthite, E: Edenite , L: Lime, Pt: Pectolite, Dl: Dellaite, Nt : Natrosilites, Et: Ertixiite.*

## 3.2 Effect of thermal treatment on molecular bonds

The FT-IR spectrums of thermally treated materials are illustrated in Figure. 10. The alumina-silicate bands Si-O-Si and Si-O-Al, have been become higher from 1046cm$^{-1}$ in untreated MK to 1058cm$^{-1}$ at 450$^{o}$C and 1078cm$^{-1}$ at 950$^{o}$C. This while the opposite to this tendency took place with the spectra of NP. This kind of shifting and enhancement of broadness of these bands, leads to the transformation of crystalline phases to an amorphous structure and high deformation in the lengths and angles of Si–O–Al and Si–O–Si bonds (Abdel-Gawwad, García, *et al.*, 2018). This transformation is satisfied by the increment of non-bridging oxygen atoms due to thermal treatment (Feng *et al.*, 2012). A considerable shifting of the C-O bond from 1402 cm$^{-1}$ to 1408cm$^{-1}$ during the treatment at 950$^{o}$C, indicates the transformation of the crystalline phase in to the glassy phase.

It can be noticed that the C-O band became wider and less intense at 950 °C spectra. The intensity reduction of this band, interprets the increment of pure CaO amounts released from $CaCO_3$.

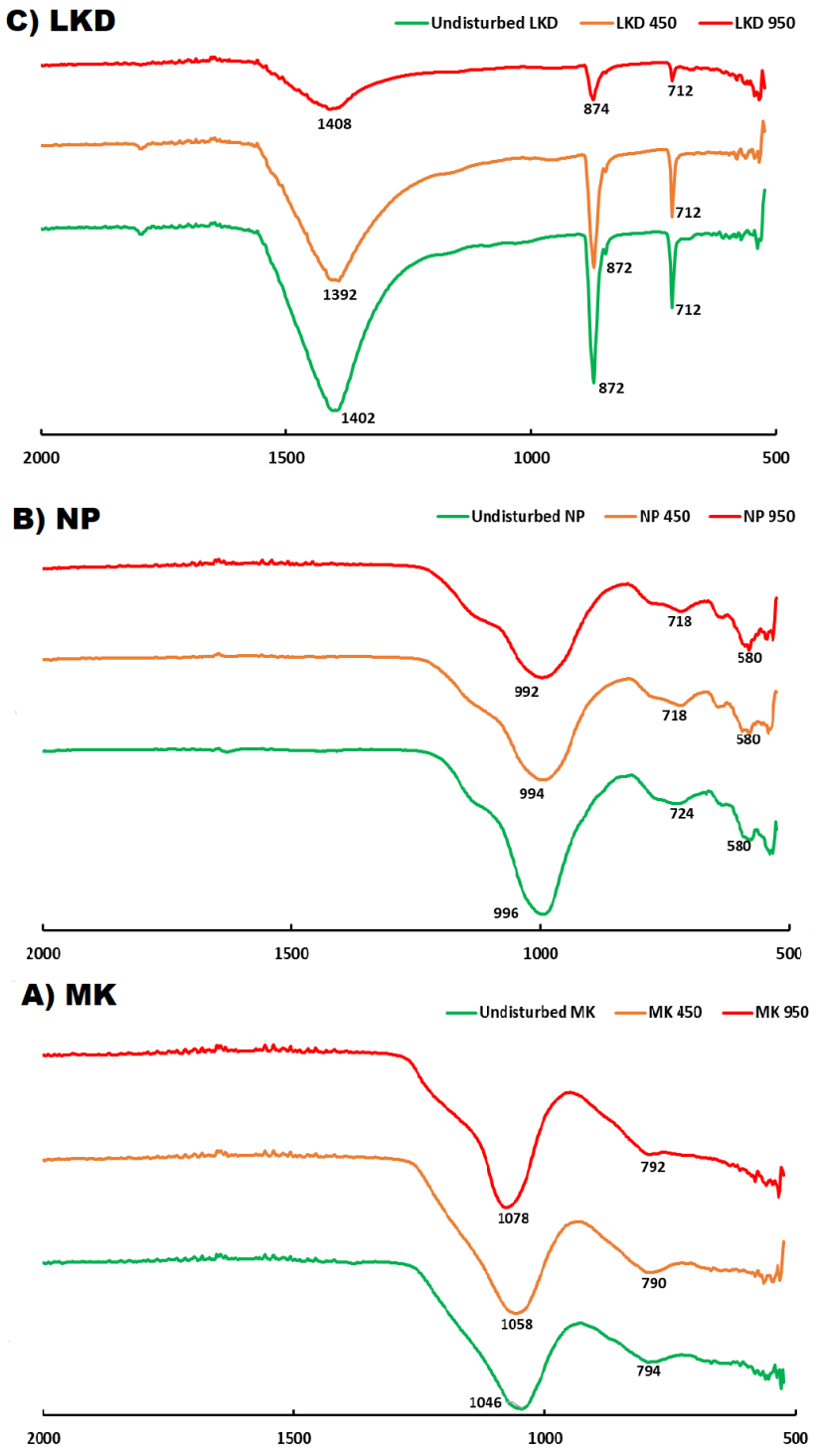


*Figure 10. FTIR spectra of materials after thermal treatment.*

## 3.3 Compressive strength

After treatment, there was a considerable increase in the compressive strength as indicated in Figure. 11. The blend containing only calcined LKD (40M40(L-950)20N) has shown a compressive strength of 24.54MPa after 28 days. The regular growth in strength of up-to 28 days for this blend indicates that hydration of raw materials was progressive with time. This development of the strength of this mix, was due to the calcination of LKD with the presence of sufficient amounts of reactive silicate and calcium oxide from the NP. A considerable amount of strength was developed within the mix, containing calcined materials individually and collectively, which has showed no cementitious properties prior to thermal treatment. Calcination at 950$^{o}$C, clearly contributed to a huge variation in LKD mineralogy and substantial reduction in its crystallinity, which was observed in the XRD patterns. In order to optimise the strength, these mortar mixes were repeated with the same procedure, but increases the proportion of NP to (35%MK 35%LKD 30%NP). The increment of the NP amount, was due to the suitable composition of NP, which contains a various range of alkaline elements including CaO, $Na_2O$ and $K_2O$, as shown in XRF results. Noticeably, the highest compressive strength was achieved at this stage with 27.3MPa in 28 days for (35M35(L-950)30N) , as shown in Figure. 11. The increment of NP weight from 20% to 30% in mortars, resulted in the growth of more C-A-S-H products. The addition of more NP contributed to extra dissolution of quartz silicate, caused by CaO and $Na_2O$ that exist in the calcined LKD and NP, yielding high binding properties. Therefore, a higher transformation to vitreous mineralogy led to a higher strength of (35M35(L-950)30N). Moreover, the fall in strength for (35M35L30N)-950) when all three components are calcined, indicated a lesser dissolution of Si/Al compounds from MK and NP, which means that less activation was caused by LKD.

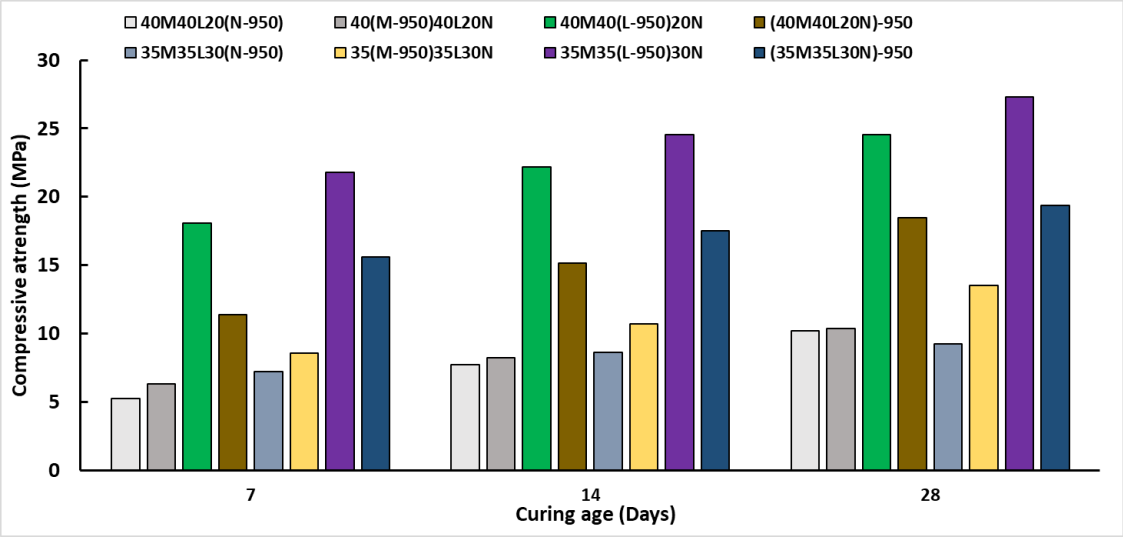


*Figure 11. Compressive strength after 950 $^{o}$C calcination.*

The TG-DTA curves have shown that the weight loss of the constituents of this ternary blend, starts at the temperatures in the range 350-500$^{o}$C. Furthermore, this was evidenced by XRD patterns, where raw materials after 450$^{o}$C treatment have displayed a considerable change in their diffraction. Therefore, the ternary blend of 35%MK 35%LKD 30%NP was formulated after 450$^{o}$C treatment with same process of mixing. The resulting compressive strength offered by the ternary bends after 450$^{o}$C treatment, has been shown in Figure. 12. A similar trend of higher strength in the case of calcining LKD individually at 450$^{o}$C, was evident in (35M35(L-450)30N) with 23.4MPa at age of 28 days. Although both early and longer-term strength were higher in the case of high temperature 950$^{o}$C treatment, no remarkable strength generation was observed compared to a lower temperature treatment (450$^{o}$C). This similar development of strength is ascribed to mineralogical and chemical changes that were noticed in both XRD and DT-TGA results, which indicated that most of diffraction patterns were starting to transform around 450$^{o}$C.

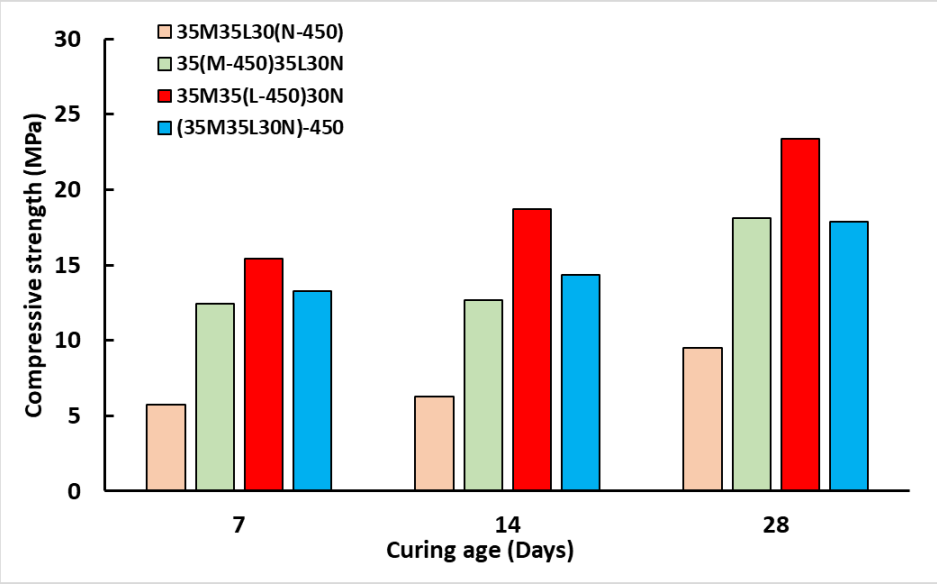


*Figure 12. Compressive strength after 450$^{o}$C calcination*

## 3.4 Reaction hydrates analysis by XRD

X-Ray diffraction (XRD) analysis, was investigated for pastes of samples with the highest strength (40M40(L-950)20N, (35M35(L-950)30N) and (35M35(L-450)30N))at age of 28 days, as presented in Figure. 13. Major hydration products can be identified and are composed chiefly of $CaO$-$Al_2O_3$-$MgO$-$SiO_2$ compounds. The utilisation of a dry alkaline (CaO) activator in the mix transforms the crystallinity diffraction patterns into amorphicity status and leads to the presence of prevailing vitreous phases. The major hydrated phases were specifically, tetra calcium aluminate hydrate; CAH ($C_4AH_{13}$); calcium aluminum silicate hydrates; St (stratlingite – $C_2ASH_8$); and Akermanite; Ak ($Ca_2MgSi_2O_7$) (Kim *et al.*, 2013)(Gameiro *et al.*, 2014)(Gameiro *et al.*, 2012)(Gameiroa *et al.*, 2011). Moreover, Gameiro (Gameiro *et al.*, 2012) stated that calcium silicate hydrate (CSH) is viewed to overlap with the lime (calcite) peak in these blends, with higher MK ($\geq$ 33% MK). XRD patterns of (40M40(L-950)20N) reveals a gentle reduction of the dominant Quartz ($SiO_2$) crystalline phase that existed in the raw MK in the range of $2\theta = 26^o$. This slight reduction indicates two facts; firstly, the remaining large amounts of this crystalline quartz are in a non-reactant status, secondly, low CaO amounts, which were less than that what was required, in order to dissolve this phase, which in terms led to less strength. However, a glassy phase of alumina-silicate gel (C-A-S-H) can be indicated in the range $2\theta$ $25^o$-$30^o$ due to the semi-amorphous nature (Escalante-García *et al.*, 2003; Elimbi *et al.*, 2014). At the same time, the strong presence of stratlingite is noticed as a permanent phase in the matrix. The formulation of stratlingite as dominant peaks in the three blends indicates that this hydrate is stable and is verified as the hydrate responsible for the enhancement of mechanical strength (Bakolas *et al.*, 2006; Gameiro *et al.*, 2012). As would be expected, crystalline quartz has decreased in (35M35(L-950)30N), as the amount of LKD was increased to 30%. The growth of stratlingite peaks can be noticed clearly through the entire range of diffraction with the increment of LKD causing higher strength for the blend. This indicates that the lime (CaO) generated from LKD has caused significant dissolution of aluminate and silicate species (Morsy *et al.*, 2017). The high amounts of MgO from NP has strongly contributed to presence of amorphous phases, such as Akermanite together with the reactive CaO from LKD. This reaction introduced new bonds such as Ca-Mg-Si, which have high contribution to the strength. $C_4AH_{13}$ was present in minor quantities due to the instability of this phase through the curing aging (Gameiro *et al.*, 2012). Additionally, portlandite ($Ca(OH)_2$) peaks were not found extensively due to the modified LKD and MK in the blends, as this peak may appear in low MK blends (Gameiro *et al.*, 2012). A range of reaction products can be noticed similarly in (35M35(L-450)30N) with LKD calcined at $450^oC$, indicating that comparative diffractions were formulated for this blend with (35M35(L-950)30N) and LKD calcined at $950^oC$. This was observed in the strength development for both levels of thermal treatment.

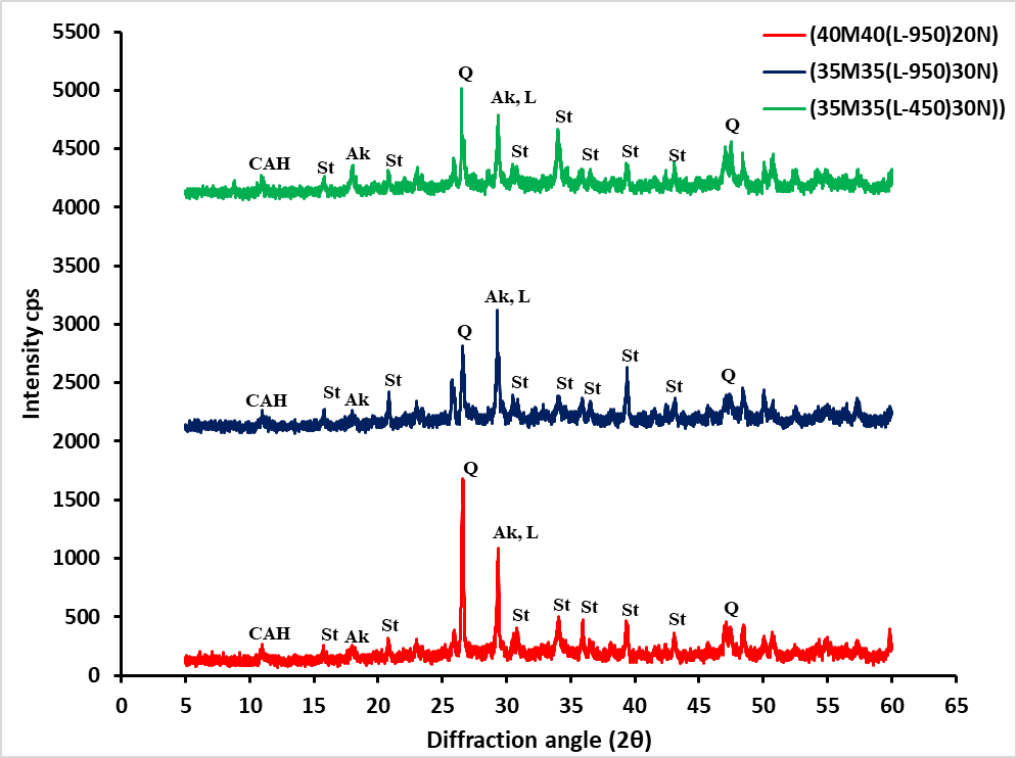


*Figure 13. XRD patterns of (40M40(L-950)20N),(35M35(L-950)30N) and (35M35(L-450)30N)) at age of 28 days.*

## 3.5 Molecular identification of hydrates by FT-IR

The FTIR spectra was reproduced for pastes with the highest compressive strength and were investigated after 28 days of curing, as shown in Figure. 14. In all spectra, the C-O band ranging from 1413,1416 and 1417 and 874,875 and 873cm$^{-1}$ were observed, and similar to infrared in the raw LKD in Figure. 14. The wide stretching band starting from 1200-900cm$^{-1}$ region of Si-O and Al-O were noticed in all the spectra of the blends. These bands reveal the strong evidence of Aft/AFm phases such as Stratlingite ($C_2ASH_8$) and Mono-Carboaluminate $Ca_4A_{l2}(CO3)(OH)_{12}$ / $_5H_2O$ (Horgnies *et al.*, 2013). A smooth shifting of Si-O and Al-O can be detected for (35M35(L-450)30N) , proving that treatment at 450ºC for LKD has contributed significantly in formulating similar bands compared to treatment at 950ºC.

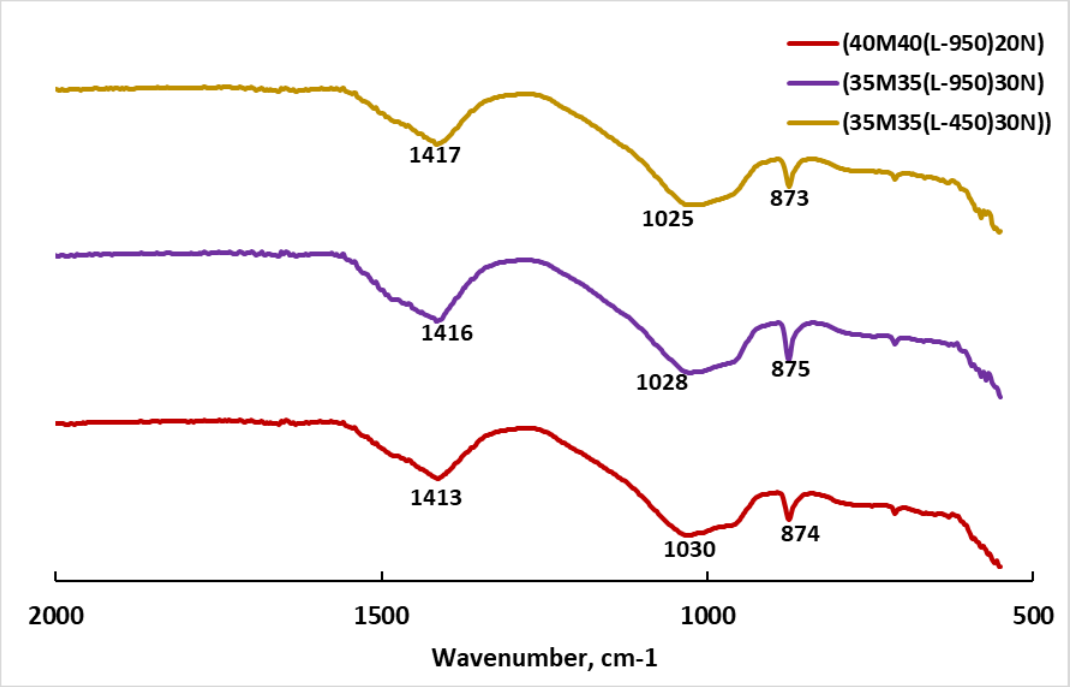


*Figure 14. FTIR-spectra of hardened pastes at age of 28 days curing.*

## 3.6 Microstructure and EDX analysis

The SEM micrographs for (40M40(L-950)20N), (35M35(L-950)30N) and (35M35(L-450)30N) at age of 28 days of curing are shown in Figure. 15. The microstructure of hardened pastes shows the prevalence of stratlingite ($C_2ASH_8$) with dense-like microstructure (Gameiroa *et al.*, 2011). The strong occurrence of $C_2ASH_8$ has specified by the appearance of rodlets of AFt phases. This illustrates the pozzolanic reaction of Si and Al with $Ca^{+2}$ cations, which encourages further dissolution and breaking the Si–O and Al–O bonds in both MK and NP (Medina *et al.*, 2016). EDX values have showed that major chemical elements include O, Al, Si and Ca; as shown in Table 5; which represent key elements responsible for the strength of blends. Moreover, minor elements were noticed such as K, Ti ,Fe and S. The Ca/Si ratio in C-A-S-H phase are similar in both (40M40(L-950)20N) and (35M35(L-950)30N) with 0.97 and 1.03 which indicates increased reaction of both elements and formation of hydrate products in the form of (stratlingite – $C_2ASH_8$)(Abdel-Gawwad *et al.*, 2019). On the opposite, Ca/Si ratio of (35M35(L-450)30N) was very high (2.71) which indicates less reaction of ($Ca^{+2}$).

509 *Table 5. Elemental composition measured by SEM/EDX*

510 *for (40M40(L-950)20N) , (35M35(L-950)30N), (35M35(L-450)30N) at age of 28 days.*

| Element(wt. %) | Mixtures | | |
|---|---|---|---|
| | **Spectrum of (40M40(L-950)20N** | **Spectrum of (35M35(L-950)30N)** | **Spectrum of (35M35(L-450)30N)** |
| **O** | 58.46 | 61.22 | 57.8 |
| **Si** | 13.95 | 13.95 | 8.94 |
| **Al** | 12.87 | 8.07 | 5.54 |
| **Ca** | 13.56 | 14.4 | 24.25 |
| **Ti** | 1.17 | 1.33 | 0 |
| **K** | 0 | 1.03 | 0.81 |
| **S** | 0 | 0 | 1.74 |
| **Fe** | 0 | 0 | 0.48 |

511

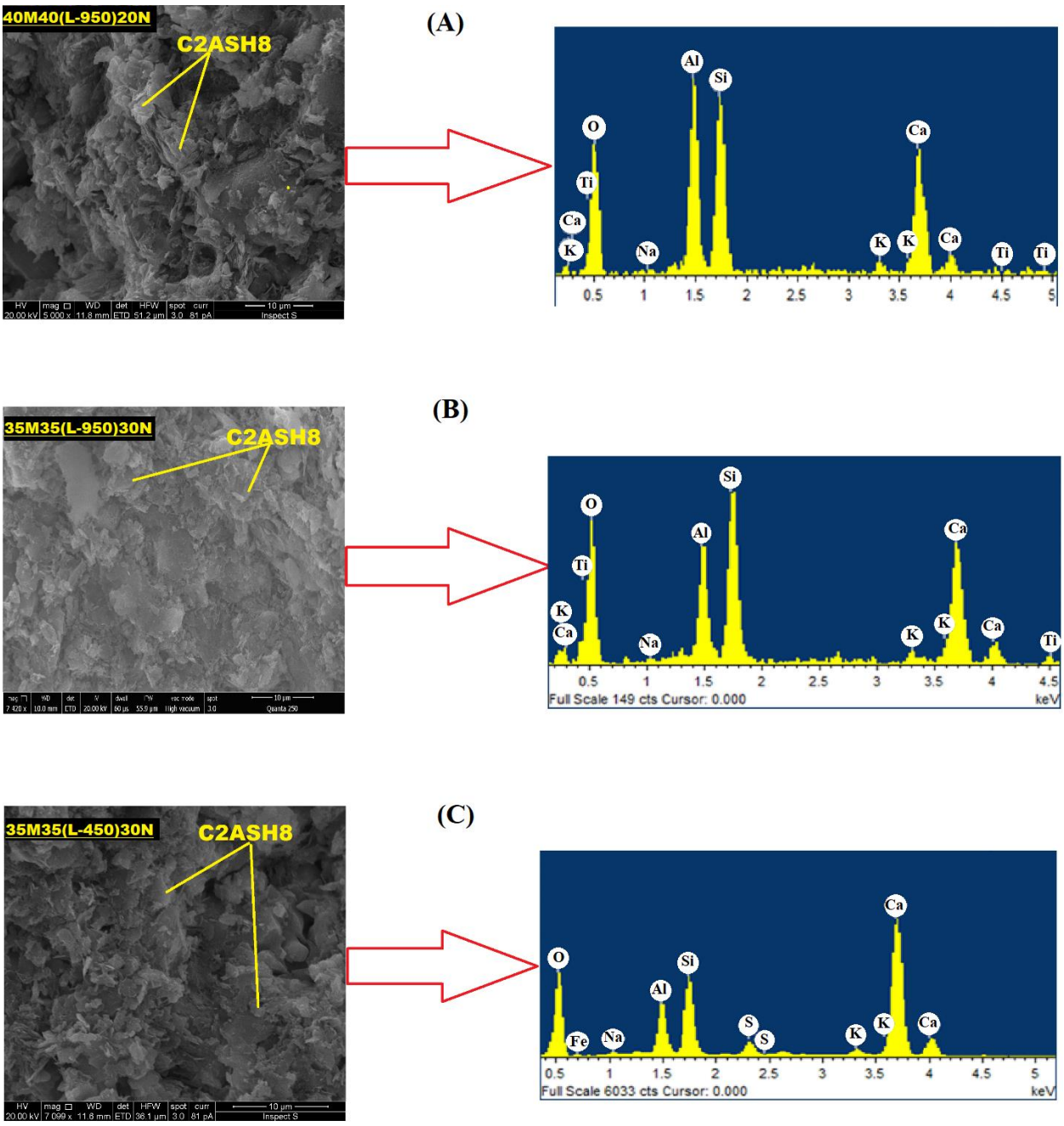


*Figure 15. SEM micrographs and EDX analysis*

*for 40M40(L-950)20N, (35M35(L-950)30N) and (35M35(L-450)30N) at age of 28 days.*

# 4. Conclusions

The research investigated the use of a waste material (Lime Kiln Dust) as a potential source of earth alkaline (CaO), for activating a combination of alumina-silicate materials to formulate one-part AAC. An assisted activation approach achieved by thermal treatment at two different temperatures (950$^{o}$C and 450$^{o}$C), was used for increasing the reactivity of materials. Comparisons were made between the performance of raw materials and thermal treatment as well as between different chosen blends by using techniques of analysis including compressive strength, XRD, TG-DTA, FTIR and SEM/EDX. The experimental investigations gave the following conclusions:

- The highest compressive strength that, was recorded is 27.3MPa at age of 28 days for mortar comprising treated LKD at 950 $^{o}$C. Comparative compressive strength was gained at 450$^{o}$C calcination level, indicating that the reactivity of materials started to increase at this temperature. The development of strength was attributed to the progressive pozzolanic reaction during the curing period.
- Thermal treatment was evidently participating in breaking the crystalline phases of the original materials and strong evidence of transformation to amorphous phases was provided by XRD, TG-DTA and FTIR results. Remarkably, this was noticed significantly at 450$^{o}$C, which saved a considerable amount of energy.
- Synthesised products characterised by XRD, FTIR and SEM/EDX methods revealed that the formation of the prevalence of hydrates responsible for the strength. These products include chiefly stratlingite ($C_2ASH_8$) and Akermanite; Ak ($Ca_2MgSi_2O_7$). XRD spectra proved that with the increment of LKD in mix, came increments of strength products formulation.
- The findings of the study, has proved that lime waste (LKD) has a high potential to be a solid alkaline activator if treated properly and its impurities are removed.


# Acknowledgement

The first author would like to acknowledge the financial support provided by the Iraqi Ministry of Higher Education and Scientific Research and the University of Babylon.

# References


Abdel-Gawwad, H. A., García, S. R. V. and Hassan, H. S. (2018) 'Thermal activation of air cooled slag to create one-part alkali activated cement', *Ceramics International*, 44(12), pp. 14935–14939.

Abdel-Gawwad, H. A. and Khalil, K. A. (2018) 'Application of thermal treatment on cement kiln dust and feldspar to create one-part geopolymer cement', *Construction and Building Materials*, 187, pp. 231–237.

Abdel-Gawwad, H. A., Rashad, A. M. and Heikal, M. (2019) 'Sustainable utilization of pretreated concrete waste in the production of one-part alkali-activated cement', *Journal of Cleaner Production*. Elsevier, 232, pp. 318–328.

Almalkawi, A. T., Hamadna, S. and Soroushian, P. (2017) 'One-part alkali activated cement based volcanic pumice', *Construction and Building Materials*, 152, pp. 367–374.

Bakolas, A. *et al.* (2006) 'Evaluationof pozzolanic activity and physicomechanical characteristics in metakaolin-limepastes', *Journal of Thermal Analysis and Calorimetry*, 84(1), pp. 157–163.

Ban, C. C., Ken, P. W. and Ramli, M. (2017) 'Mechanical and Durability Performance of Novel Self-activating Geopolymer Mortars', *Procedia Engineering*, 171(Supplement C), pp. 564–571.

British Standard Institution (BSI) (2010) *196-6: 2010, Methods of testing cement, Determination of fineness, London, England: British Standard Institution (BSI)*. London: BSI Standards Limited.

British Standard Institution (BSI) (2016) *196-1: 2016, Methods of Testing Cement, Determination of Strength, London, England: British Standard Institution (BSI)*. London: BSI Standards Limited.

Cabrera, J. and Rojas, M. F. (2001) 'Mechanism of hydration of the metakaolin–lime–water system', *Cement and Concrete Research*. Elsevier, 31(2), pp. 177–182.

Davidovits, J. (1993) 'Geopolymer cements to minimise carbon-dioxide greenhouse-warming', *Ceram. Trans.*, 37, pp. 165–182.

Davidovits, J. (2017) 'Geopolymers based on natural and synthetic metakaolin-A critical review', *on Advanced Ceramics and Composites*. Wiley Online Library, 38(3), p. 201.

Demie, S., Nuruddin, M. F. and Shafiq, N. (2013) 'Effects of micro-structure characteristics of interfacial transition zone on the compressive strength of self-compacting geopolymer concrete', *Construction and Building Materials*, 41, pp. 91–98.

Van Deventer, J. S. J., Provis, J. L. and Duxson, P. (2012) 'Technical and commercial progress in the adoption of geopolymer cement', *Minerals Engineering*, 29(Supplement C), pp. 89–104.

Duxson, P., Lukey, G. C. and van Deventer, J. S. J. (2007) 'Physical evolution of Na-geopolymer derived from metakaolin up to 1000 C', *Journal of Materials Science*. Springer, 42(9), pp. 3044–3054.

Eilers, L. H., Nelson, E. B. and Moran, L. K. (1983) 'High-temperature cement compositions-pectolite, scawtite, truscottite, or xonotlite: which do you want?', *Journal of Petroleum Technology*. Society of Petroleum Engineers, 35(07), pp. 1–373.

Elimbi, A. *et al.* (2014) 'Thermal behavior and characteristics of fired geopolymers produced from local Cameroonian metakaolin', *Ceramics International*. Elsevier, 40(3), pp. 4515–4520.

588 Escalante-García, J. I. *et al.* (2003) 'Hydration Products and Reactivity of Blast-Furnace Slag
589 Activated by Various Alkalis', *Journal of the American Ceramic Society*. Wiley Online Library,
590 86(12), pp. 2148–2153.

591 Feng, D., Provis, J. L. and van Deventer, J. S. J. (2012) 'Thermal Activation of Albite for the
592 Synthesis of One-Part Mix Geopolymers', *Journal of the American Ceramic Society*. John Wiley
593 & Sons, Ltd (10.1111), 95(2), pp. 565–572.

594 Gameiro, A. *et al.* (2012) 'Hydration products of lime–metakaolin pastes at ambient temperature
595 with ageing', *Thermochimica Acta*, 535, pp. 36–41.

596 Gameiro, A. *et al.* (2014) 'Physical and chemical assessment of lime–metakaolin mortars:
597 Influence of binder:aggregate ratio', *Cement and Concrete Composites*, 45, pp. 264–271.

598 Gameiroa, A. *et al.* (2011) 'Metakaolin-Lime Hydration Products and Phase Stability: A
599 Microscopy Analysis', *BOOK OF EXTENDED*, p. 31.

600 Garbev, K. *et al.* (2008) 'First Observation of α-Ca2 [SiO3 (OH)](OH)–Ca6 [Si2O7][SiO4](OH)
601 2 Phase Transformation upon Thermal Treatment in Air', *Journal of the American Ceramic*
602 *Society*. Wiley Online Library, 91(1), pp. 263–271.

603 He, P. *et al.* (2010) 'Effect of cesium substitution on the thermal evolution and ceramics formation
604 of potassium-based geopolymer', *Ceramics International*. Elsevier, 36(8), pp. 2395–2400.

605 Heath, A. *et al.* (2013) 'The potential for using geopolymer concrete in the UK', *Proceedings of*
606 *the Institution of Civil Engineers: Construction Materials*, 166(4), pp. 195–203.

607 Hill, J. O. and Verma, R. K. (2019) 'Thermal Analysis | Coupled Techniques☆', in Worsfold, P.
608 et al. (eds). Oxford: Academic Press, pp. 6–11.

609 Horgnies, M., Chen, J. J. and Bouillon, C. (2013) 'Overview about the use of Fourier Transform
610 Infrared spectroscopy to study cementitious materials', *WIT Transactions on Engineering*
611 *Sciences*, 77, pp. 1743–3533.

612 Ilić, B. R., Mitrović, A. A. and Miličić, L. R. (2010) 'Thermal treatment of kaolin clay to obtain
613 metakaolin', *Hemijska industrija*, 64(4), pp. 351–356.

614 Justnes, H. *et al.* (1990) 'Nuclear magnetic resonance (NMR)—a powerful tool in cement and
615 concrete research', *Advances in Cement Research*. Thomas Telford Ltd, 3(11), pp. 105–110.

616 Kakali, G. *et al.* (2001) 'Thermal treatment of kaolin: the effect of mineralogy on the pozzolanic
617 activity', *Applied Clay Science*, 20(1), pp. 73–80.

618 Kim, M. S. *et al.* (2013) 'Use of CaO as an activator for producing a price-competitive non-cement
619 structural binder using ground granulated blast furnace slag', *Cement and Concrete Research*, 54,
620 pp. 208–214.

621 Kimata, M. *et al.* (1996) 'Anorthite megacrysts from island arc basalts', *Oceanographic Literature*
622 *Review*, 1(43), p. 50.

623 Li, C., Sun, H. and Li, L. (2010) 'A review: The comparison between alkali-activated slag (Si+
624 Ca) and metakaolin (Si+ Al) cements', *Cement and Concrete Research*. Elsevier, 40(9), pp. 1341–
625 1349.

626 Li, X., Wang, Z. and Jiao, Z. (2013) 'Influence of curing on the strength development of calcium-

containing geopolymer mortar', *Materials*. School of Civil Engineering, Harbin Institute of Technology, Harbin 150006, China, 6(11), pp. 5069–5076.

Licht, S. (2016) 'Process for synthesis of calcium oxide'.

Luukkonen, T. *et al.* (2018) 'One-part alkali-activated materials: A review', *Cement and Concrete Research*. Elsevier, 103, pp. 21–34.

Matalkah, F. *et al.* (2016) 'Mechanochemical synthesis of one-part alkali aluminosilicate hydraulic cement', *Materials and Structures*, 50(1), p. 97.

Medina, C. *et al.* (2016) 'Mineralogy and microstructure of hydrated phases during the pozzolanic reaction in the sanitary ware waste/Ca (OH) 2 system', *Journal of the American Ceramic Society*. Wiley Online Library, 99(1), pp. 340–348.

Miguel, G.-R. *et al.* (2009) 'Characterization of Calcium Carbonate, Calcium Oxide, and Calcium Hydroxide as Starting Point to the Improvement of Lime for Their Use in Construction', *Journal of Materials in Civil Engineering*. American Society of Civil Engineers, 21(11), pp. 694–698.

Miller, M. M. and Callaghan, R. M. (2004) 'Lime Kiln Dust as a Potential Raw Material in Portland Cement Manufacturing'.

Mineralproducts.org (2017) 'Novel cements: low energy, low carbon cements'. Mineralproducts.org.

Morsy, M. S. *et al.* (2017) 'Mechanical properties, phase composition and microstructure of activated Metakaolin-slaked lime binder', *KSCE Journal of Civil Engineering*. Springer, 21(3), pp. 863–871.

Nath, P. and Sarker, P. K. (2015) 'Use of OPC to improve setting and early strength properties of low calcium fly ash geopolymer concrete cured at room temperature', *Cement and Concrete Composites*. Elsevier, 55, pp. 205–214.

Nayak, P. S. and Singh, B. K. (2007) 'Instrumental characterization of clay by XRF, XRD and FTIR', *Bulletin of Materials Science*. Springer, 30(3), pp. 235–238.

Peng, M. X. *et al.* (2017) 'Effects of alkali on one-part alkali-activated cement synthesized by calcining bentonite with dolomite and Na2CO3', *Applied Clay Science*. School of Materials Science and Engineering, Hunan University of Science and Technology, Xiangtan, China, 139, pp. 64–71.

Perera, D. S. *et al.* (2007) 'Influence of curing schedule on the integrity of geopolymers', *Journal of materials science*. Springer, 42(9), pp. 3099–3106.

'Production of purified calcium carbonate' (1993).

Provis, J. L. (2014) 'Introduction and scope', *RILEM State-of-the-Art Reports*. Department of Materials Science and Engineering, University of Sheffield, Sheffield, United Kingdom, pp. 1–9.

Provis, J. L. (2017) 'Alkali-activated materials', *Cement and Concrete Research*.

Provis, J. L. and Bernal, S. A. (2014) 'Geopolymers and related alkali-activated materials', *Annual Review of Materials Research*. Annual Reviews, 44, pp. 299–327.

Provis, J. L., Palomo, A. and Shi, C. (2015) 'Advances in understanding alkali-activated materials', *Cement and Concrete Research*, 78.

Ramachandran, V. S. and Beaudoin, J. J. (2000) *Handbook of analytical techniques in concrete science and technology: principles, techniques and applications*. Elsevier.

Rashad, A. M. (2013) 'Metakaolin as cementitious material: History, scours, production and composition – A comprehensive overview', *Construction and Building Materials*, 41, pp. 303–318.

Rashad, A. M., Hassan, A. A. and Zeedan, S. R. (2016) 'An investigation on alkali-activated Egyptian metakaolin pastes blended with quartz powder subjected to elevated temperatures', *Applied Clay Science*, 132–133, pp. 366–376.

Sanz, J. *et al.* (1988) 'Aluminum-27 and Silicon-29 magic-angle spinning nuclear magnetic resonance study of the kaolinite-mullite transformation', *Journal of the American Ceramic Society*. Wiley Online Library, 71(10), pp. C418–C421.

Singh, B. *et al.* (2015) 'Geopolymer concrete: A review of some recent developments', *Construction and building materials*. Elsevier, 85, pp. 78–90.

Torres-Carrasco, M. and Puertas, F. (2017) 'Alkaline activation of different aluminosilicates as an alternative to Portland cement: alkali activated cements or geopolymers', *Revista Ingeniería de Construcción*, 32(2), pp. 5–12.

U.S. Geological Survey (2019) *Mineral commodity summaries 2019*. Virginia.

Vaccari, M., Gialdini, F. and Collivignarelli, C. (2013) 'Study of the reuse of treated wastewater on waste container washing vehicles', *Waste management*. Elsevier, 33(2), pp. 262–267.

Vizcayno, C. *et al.* (2010) 'Pozzolan obtained by mechanochemical and thermal treatments of kaolin', *Applied Clay Science*. Elsevier, 49(4), pp. 405–413.

Weerdt, K. De (2011) *Geopolymers – State of the art*. Blindern.

Yao, X. *et al.* (2009) 'Geopolymerization process of alkali–metakaolinite characterized by isothermal calorimetry', *Thermochimica Acta*. Elsevier, 493(1–2), pp. 49–54.

# List of Figures



# List of Tables